



Research paper

A mathematical model for the dynamic analysis of multi-body floating platforms with complex mechanical constraints

Thiago S. Hallak, José F. Gaspar, C. Guedes Soares^{*}

Centre for Marine Technology and Ocean Engineering (CENTEC), Instituto Superior Técnico, Universidade de Lisboa, Lisbon, Portugal

ARTICLE INFO

Keywords:

Multi-body hydrodynamics
Offshore renewable energy
Floating offshore wind turbine
Floating wind-wave platform
Nonlinear mechanics
Time domain simulation

ABSTRACT

The new methodology based on generalised coordinates for the analysis of floating multi-body systems with nonlinear geometric constraints is developed, and it is demonstrated through numerical application for a hybrid floating wind-wave platform consisting of a floating offshore wind turbine and an articulated wave energy converter that moves a hydraulic piston. The formulation is applied to achieve explicit formulae regarding the dynamic response in a low-dimensional scenario used to verify a post-processing code. The verification considers the nonlinear geometric constraints, hydrodynamic interaction, the dynamics of articulated arms, and the dynamics of hydraulic power take-off systems. An analytical expression for the system's natural frequencies is attained and verified likewise. The results presented in this paper indicate significant improvement in the simulation and analysis of multi-degrees-of-freedom nonlinear hydrodynamic systems, which will ultimately be necessary for designing efficient hybrid floating wind-wave platforms.

1. Introduction

The theoretical analysis of floating systems with multiple underwater geometries started over 50 years ago; however, the application was somewhat limited to rigid-body structures with multiple underwater geometries, such as the case of catamarans and floating stations (Ohkusu, 1969). Nevertheless, important conclusions were drawn regarding interactions between the different hulls, for instance, those interactions may be exceptionally strong for specific wavelengths and spacing between hulls (Ohkusu, 1970).

The theoretical analysis of floating systems with separated geometries started years later, at the beginning of the 1970s, and with direct application in problems of ship-to-ship interactions, especially the ones raised by passing ships near moored ships in ports (Tuck and Newman, 1974; Yeung, 1978). The studies were conducted after a series of accidents at sea, but the matter still has importance in research and practical engineering (Zhou et al., 2021; Xu et al., 2024).

The theoretical analysis of floating multi-body systems for offshore renewable energy (ORE) application started not much later, as one may think. Indeed, the generalisation of hydrodynamic wave-structure interaction formulation was first demonstrated for multi-body systems with many geometries (Budal, 1977; Falnes, 1980), within a theory that had direct application in farms of wave energy converters (WECs). At the

time, however, the application was somewhat limited to identical and axisymmetric bodies, yet knowledge acquired during years of investigation led to several contributions to the field of multi-body hydrodynamics (e.g., Mavrakos, 1991; McIver, 1994; Mavrakos and McIver, 1997; Mavrakos and Kalofonos, 1997). Today, the state-of-the-art hydrodynamic modelling for WECs and WEC arrays encompasses many robust techniques, especially for optimisation (e.g., Fitzgerald and Thomas, 2007; Child and Venugopal, 2010; Sinha et al., 2016b) and control strategies (e.g., Balitski et al., 2014; Gaspar et al., 2017).

The effects of wave multi-scattering raised by floating multi-modules or multi-body structures have been detailed and applied to different structures by Chakrabarti (1999, 2000). Though the latter scholar has introduced a powerful modelling technique, there is a lack of in-depth research that validates multi-scattering wave models for a series of floating multi-modules or multi-body structures. In the case of constrained floating multi-body structures, theoretical analysis started near the 1990s, when it was demonstrated that the usual formulation of first-order wave-structure interaction can be applied to hinged structures using generalised modes formulation (Newman, 1994). Newman (2001) has also reviewed and summarised the many conclusions drawn by the different floating multi-body modelling techniques, emphasising the wave field's near-trapping modes within WEC arrays. Time domain simulation of floating multi-body geometries with hydrodynamic

^{*} Corresponding author.

E-mail address: c.guedes.soares@centec.tecnico.ulisboa.pt (C. Guedes Soares).

interaction has been studied in detail by Kara (2020), who demonstrated that the influence of the coupled impulse response functions (IRFs) depends on the relative distance between different floating bodies.

More recently, the research on multi-body hydrodynamics has become important again, with particular emphasis on constrained floating multi-body structures, due to the economic trends of offshore aquaculture (Mohapatra et al., 2021; Liu and Guedes Soares, 2023) and, especially, the rapid development of floating offshore wind (Diaz and Guedes Soares, 2020; GWEC – Global Wind Energy Council, 2024). The number of FOWTs in operation is expected to increase significantly in years to come (Diaz et al., 2022).

Thus, today, research on hybrid platforms for ORE extraction offshore is seen as a hot topic, where the recent developments in floating wind-wave platforms (FWWPs) have been reviewed by Hallak and Guedes Soares (2024). For instance, it is concluded that prospective hybrid systems are the ones based on multi-WEC arrangements or massive displacement hulls (e.g., Asai et al., 2024; Stansby and Li, 2024), though the structural integrity of the latter designs has not been assessed. It is shown that single-WECs employed on available FOWT designs do not lead to significant cost-savings nor additional energy output, whereas the main advantages to be explored with the coupling are an increase in weather windows for operation & maintenance (O&M) in the farm – as proven by Teixeira-Duarte et al. (2024), and the reduction of intermittency and smoother energy output – as demonstrated by Gao et al. (2024). It is also concluded that, for various FWWP configurations, WECs may be actively and accurately controlled to suppress system loads and reduce wind turbine accelerations and fatigue loads, to increase the FOWTs' lifetime. This will depend on rational design and optimisation at different levels, which is currently a research gap within the field.

Besides hydrodynamic effects, the physical complexity of floating multi-body systems is further increased when mechanical connections are considered, which is the case of FWWPs. Mechanical connections may be performed using mechanical bearings, flexible connectors, joints, and articulated arms, among others, whereas the constraint forces that appear in the connection point are hard to control, and the constraint equations may be nonlinear, as is the case of articulated arms. The constraints may also require the application of Gauss' Principle of Least Constraint to be correctly modelled, even though the mathematical models used for FWWPs are still based on the classical Newtonian perspective. For instance, Chen et al. (2023) studied floating multi-body hydrodynamics from the perspective of flexible interconnections: A robust mathematical model was developed and used for frequency and time domain analysis of various types of flexible floating multi-body systems. The major drawback of the model is that the interconnections are simplified – they are performed by single-point flexible connectors, which is not realistic for the PTO models.

Zhao et al. (2021) developed a semi-analytical formulation for the performance of a WEC mounted on a floating breakwater near the seawall. This model is robust and accounts for all main interactions between waves, floating breakwater, and the WEC. The model was later extended for WEC arrays mounted on flexible platforms (Zhao et al., 2023). The results are promising, showing that the model is one of the few hydrodynamic models that accounts for the complex dynamics of PTOs when mounted on top of floating platforms. In these studies, however, the major drawback comes from the two-dimensional modelling, which is suitable for floating breakwaters but unsuitable for hybrid wind-wave technologies or hydrodynamic systems under short-crested sea waves.

Some FWWP configurations represent reduced complexity in terms of dynamic behaviour. That is particularly true for the Spar-Torus Combination (STC), which has been intensely studied in the literature and validated in the laboratory (Wan et al., 2015, 2016). Because only one WEC is employed and only one extra DOF is added to the dynamic system (namely, the relative heaving mode), both mathematical and physical complexities are reduced, while in practice, the STC would be

accomplished using shafts. Results presented by different studies that further investigated the STC reveal that the heaving motion of the spar is drastically increased after coupling it to the torus WEC (e.g., Li et al., 2018; Skene et al., 2021).

The platform investigated in this paper belongs to another configuration deeply studied in the literature: The combination of a semi-submersible FOWT with point absorber (PA) WECs. The general concept enables different possible configurations and WEC arrangements; thus, many configurations have been addressed in the literature, but the research is mostly preliminary and has not converged to an ideal FOWT-PA-WEC geometry. Possibilities include, for instance, the coupling between a semi-submersible FOWT with articulated PA-WECs hinged on the bracings of the platform, a configuration that has been through experimental validation, as provided in detail by Sinha et al. (2016a) and Kamarlouei et al. (2020, 2022) for a series of arrangements with different number of WECs, spring and damping components. Numerical analyses of similar configurations are given by Ghafari et al. (2021, 2022), where it is shown that maximum wave power absorption is found at around 10-m diameter WECs for this particular configuration.

For articulated PA-WECs hinged on the columns of the platform, numerical analysis has been conducted for different configurations by Hallak et al. (2021), Si et al. (2021), and Wu et al. (2024). By comparing the results provided by the different references, it is noted that the configurations with hinges on the bracings can be more advantageous than the hinges on the columns because when the WECs are closer to the platform's Centre of Gravity (CoG), the lever effects that influence pitch motion are reduced.

Other configurations have been analysed, for instance, heaving WECs below the FOWT bracings (e.g., Hu et al., 2020; Chen et al., 2022; Zhu et al., 2023), and heaving WECs on a modified superstructure to accommodate the WECs and PTO near the middle of the platform (e.g., Chen et al., 2020; Chen et al., 2024). By comparing the different references, it is concluded that heaving WECs, especially near the middle of the platform, are much less likely to modify the dynamics of the hybrid platform than articulated WECs. However, articulated WECs can provide more stability and absorb more wave power.

The state-of-the-art multi-body hydrodynamic models for articulated geometries usually violate the nonlinear mechanical constraints imposed by actual PTOs and articulated arms. Despite the modelling issues, articulated point absorbers provide the highest energy absorption per unit of mass, around 1.5 MWh/ton, as revealed by a benchmark study on eight types of WECs performed by Babarit et al. (2012). That is a benefit when coupling WECs with FOWTs, for the maximum deck load on an FOWT might not be too high. The trade-off appears on the PTO forces, which are high overall, quickly reaching the order of 10^4 kN. The mathematical formulation presented by Hallak et al. (2023) has been developed to overcome the modelling issues of articulated floating multi-body geometries and hydraulic PTOs that single-point PTO models cannot represent.

This paper extends the formulation and applies it to a realistic case study, a hybrid ORE system that combines an adapted version of the DeepCWind semi-submersible platform for a 10 MW wind turbine with a nonlinear articulated point absorber WEC. Explicit formulae are achieved for the dynamic response of the different floating bodies and the system's natural frequencies. Also, a post-processing tool is verified by comparing numerical results with analytical formulae. Moreover, the response amplitude operators (RAOs) and response phase operators (RPOs) of the combined system, are obtained and analysed in detail, as well as the wave power absorption characteristics.

The paper is organised as follows: Section 2 presents the mathematical model in detail, including the theoretical assumptions and the evaluation of responses and natural frequencies. Section 3 describes the mathematical-numerical model implementation within the hybrid ORE case study, including the environmental parameters. Section 4 presents analytical and numerical results and a detailed analysis of the obtained results. Finally, in Section 5, the several conclusions obtained from the

investigation are drawn and further discussed.

2. Mathematical modelling

2.1. Potential flow theory

Despite its limitations, potential flow theory has evolved within the field of hydrodynamics as a relatively straightforward theory. Within this theory, many physical phenomena and constraints are respected, such as the conservation of mass and momentum, the boundary conditions (some exactly, others in linearised form) and the dispersion of ocean waves, to cite a few. Due to such representativeness, potential flow theory can devise reasonable wave-structure interaction models for large fixed and floating offshore structures and displacement hulls.

The development of potential flow theory has yielded textbooks, e.g., Newman (1977), making it solid. A generalisation of the same theory has been proven sound for floating multi-body geometries, while it is mainly based on the linear separation of potentials and exact definition of the multi-body geometries. That said, this paper will not discuss the basis of the potential flow theory found in Newman (1977). The theory will now be applied to the particular case of wave-structure interaction for floating constrained multi-body geometries.

2.2. Frequency domain formulation

Because the hydrodynamic loads in wave-structure interaction come from the environment, they are normally evaluated from a global perspective. Thus, the global reference frame O_{xyz} is used to define the global motion variables. The global reference frame is centred in the waterplane ($z = 0$), with the z -axis pointing upwards.

Within a frequency domain formulation, it is further assumed that the potentials can be linearly separated, that is, diffraction effects are modelled as if the floating bodies were at rest, and the radiation effects are modelled as if there were no other perturbations in the wave field. The diffraction potential is proportional to the wave amplitude, while the radiation potentials are proportional to the motion amplitudes. The effects of multi-scattering are not accounted for, meaning that one body's diffracted or radiated waves do not perturb the other bodies. Then, the total velocity potential Φ can be split as the wave field,

$$\Phi \equiv \Phi(\mathbf{F}, t) = |\Phi(\mathbf{F})| \exp i\omega t = \Phi_{\text{exc}} + \Phi_{\text{rad}} = A_w (\Phi_{\text{inc}} + \Phi_{\text{diff}}) + \sum_{i=1}^N \sum_{j=1}^6 \xi_{ij} \Phi_{\text{rad}ij}, \quad (1)$$

where ω is the wave frequency, \mathbf{F} is the position vector of the fluid particle, Φ is the total velocity potential, Φ_{exc} is the exciting potential, Φ_{inc} the incident wave potential, Φ_{diff} is the diffracted wave potential,

$$f_{ci} = H_i \left(\mathbf{w}_1, \dot{\mathbf{w}}_1, \ddot{\mathbf{w}}_1, \dots, \mathbf{w}_{6N-K}, \dot{\mathbf{w}}_{6N-K}, \ddot{\mathbf{w}}_{6N-K}, \mathbf{y}_1, \dots, \mathbf{y}_K \right) = \sum_{j=1}^{6N-K} \left(h_{ij}^{(0)} \mathbf{w}_j + h_{ij}^{(1)} \dot{\mathbf{w}}_j + h_{ij}^{(2)} \ddot{\mathbf{w}}_j \right) + \sum_{j=1}^K h_{i(6N-K+j)} \mathbf{y}_j, \quad i = 1, \dots, 6N, \quad (6)$$

Φ_{rad} is the total radiation potential, N is the number of floating bodies, A_w is the amplitude of the incoming wave, and ξ_{ij} is the amplitude of motion of the body i in mode j .

The velocity of a fluid particle is given by the real part of the gradient of the total potential,

$$\mathbf{v}(\mathbf{F}, t) = \text{Re}\{\nabla(\Phi(\mathbf{F}, t))\}. \quad (2)$$

2.3. Equation of motion

The hydrodynamic problem of wave-structure interaction between

planar Airy waves and a rigid-body structure is physically represented by a mass-spring-damper system or, mathematically, by a 2nd-order linear ordinary differential equation (ODE). For a single rigid body, if all modes of motion are considered, the dimension of the ODE system is six. If different floating structures are considered, a first generalisation is obtained by increasing the linear system's dimension and the DOF number accordingly. Further addition of constraints may reduce the number of DOFs in the system, but not necessarily the number of variables. If the constraint equations are holonomic, as in the case of articulated arms, then the equations of motion may be obtained with the Newton-Euler method.

Under these assumptions, the dynamic equation of the multi-body system can be written as

$$[M + M_{\text{rad}}(\omega)]\{\ddot{\mathbf{x}}\} + [B_{\text{add}} + B_{\text{rad}}(\omega)]\{\dot{\mathbf{x}}\} + [C_{\text{hyds}}]\{\mathbf{x}\} = \{f_e(\omega)\} + \{f_c\}, \quad (3)$$

where M is the mass-inertia matrix, $M_{\text{rad}}(\omega)$ is the added mass matrix obtained from the radiation potential, $B_{\text{rad}}(\omega)$ is the radiation damping matrix, B_{add} is the added damping matrix, C_{hyds} is the hydrostatic restoring matrix, \mathbf{x} are the global coordinates, $f_e(\omega)$ is the wave excitation force array and f_c is the constraint force array.

If the different bodies are connected through an articulated arm, in terms of the variables \mathbf{x} , the geometric constraint imposed, though holonomic, is nonlinear, for the following quantity must be constant,

$$L_{PQ} \equiv \|\mathbf{P}, \mathbf{Q}\| \Rightarrow (L_{PQ})^2 = (x_P - x_Q)^2 + (y_P - y_Q)^2 + (z_P - z_Q)^2, \quad (4)$$

where $\mathbf{P} = (x_P, y_P, z_P)$ and $\mathbf{Q} = (x_Q, y_Q, z_Q)$ are the position vectors of the interconnection endpoints (hinged or fixed connections) and L_{PQ} is the length of the arm.

2.4. Multi-body hydrodynamics – modelling of constrained systems

The nonlinear system of equations is analytically and numerically demanding to solve. The formulation presented by Hallak et al. (2023) is herein considered to obtain the equation of motion in a constrained scenario. The formulation is based on generalised coordinates, i.e., a set of parameters is used to represent the state of the multi-body system, whereas in the devised formulation both motion DOFs and constraint forces may be taken as variables.

Then, generalised DOFs and forces are taken by considering linear combinations G, H , s.t.,

$$\mathbf{x}_i = G_i(\mathbf{w}_1, \mathbf{w}_2, \dots, \mathbf{w}_{6N-K}) = \sum_{j=1}^{6N-K} g_{ij} \mathbf{w}_j, \quad i = 1, \dots, 6N, \quad (5)$$

and

where N is the number of floating bodies, K is the number of constraints, \mathbf{w}_j is the j -th generalised coordinate, g_{ij} is the coefficient of the linear combination G_i representing the influence of generalised coordinate j on global motion i , f_{ci} is the constraint force on global motion i , y_j is the j -th generalised force, $h_{i(6N-K+j)}$ is the coefficient of linear combination H_i representing the influence of generalised force j on the constraint force i and $h_{ij}^{(k)}$ is the coefficient of the linear combination H_i representing the influence of k -th derivative of the generalised motion j on the constraint force i .

The substitution of Eqs. (5) and (6) back into Eq. (3) leads to the $6N \times$

6N linear system,

$$[A]\{\ddot{w}, \dot{y}\} + [B]\{\dot{w}, y\} + [C]\{w, y\} = \{f_c(\omega)\}, \quad (7)$$

where

$$a_{ij} \equiv a_{ij}(\omega) = \sum_{k=1}^{6N} (m_{ik} + m_{radik}(\omega))g_{kj} - h_{ij}^{(2)}, \quad (8)$$

$$b_{ij} \equiv b_{ij}(\omega) = \sum_{k=1}^{6N} (b_{addik} + b_{radik}(\omega))g_{kj} - h_{ij}^{(1)}, \quad (9)$$

$$c_{ij} = \sum_{k=1}^{6N} c_{hydsik}g_{kj} - h_{ij}^{(0)} - h_{ij}, \quad (10)$$

are the coefficients of matrixes A , B and C .

According to Eqs. (5) and (6),

$$g_{ij}, h_{ij}^{(1)}, h_{ij}^{(2)} = 0, \forall j > 6N - K. \quad (11)$$

Thus, the last K columns of matrixes A and B are null, meaning that the equation of motion has no term proportional to the derivatives of the constraint forces, \dot{y} and \dot{y} , whereas in the last K columns of C appear the generalised force coefficients h_{ij} .

Remarkably, the coefficients in Eqs. (8)–(11) may be derived considering different types of mechanical joints at point Q .

2.5. Articulated arm and hydraulic PTO

This sub-section devises formulae for a particular hydraulic system that connects different floating bodies with many supporting points for a special application in a hybrid FWWP platform. Different evaluations will likely be required for other types of mechanical connections.

Fig. 1 depicts the articulated arm and hydraulic PTO systems considered about the FOWT and PA-WEC it connects. Though the FOWT and WEC are still not defined, all relevant geometric parameters of the articulated arm are presented.

In Fig. 1, the local, CoG-based reference frames are shown and are represented by C_{XYZ} and $C_{X'Y'Z'}$ for the FOWT and WEC, respectively. Each floating body's 6 DOF motion (surge, sway, heave, roll, pitch and yaw) is defined around those frames in the conventional manner, where the right-hand rule defines rotations. The translated global reference frame $O_{x'y'z'}$ is a third kind of reference frame represented in Fig. 1, and it is helpful to account for the phase difference of the incoming waves encountering different floating bodies. Moreover, WEC's CoG is represented at the same height as the waterline ($z = 0$), thus $O_{x'y'z'}$ coincides with $C_{X'Y'Z'}$. However, that is not a requirement for using the method.

The PTO is assumed to be aligned with the z -axis. Then, the vertical contact force acting on the platform around the PTO is given by the reaction of the force acting on the piston, that is,

$$f_{PTO_z} = \mu \ddot{w}_{PTO} + \beta \dot{w}_{PTO} + \kappa w_{PTO}, \quad (12)$$

where μ is the inertial parameter of the PTO, also accounting for supplementary mass, β is the PTO damping coefficient, and κ is the PTO stiffness coefficient.

In the frequency domain, the power absorbed by the WEC is given by

$$P(\omega) = \frac{1}{2} \beta (\omega W_{PTO})^2, \quad (13)$$

where $W_{PTO} \equiv W_{PTO}(\omega)$ is the motion amplitude of the hydraulic piston.

2.6. Low-dimensional multi-body scenario

For verification, further simplification is achieved by neglecting the y -dimension, and considering inactive surge modes. Then, the number of DOFs is reduced to three, namely, the heaving mode (generalised mode w_H), the pitching mode (w_P), and the relative motion between the different floating bodies, which is defined by w_{PTO} , i.e., the displacement of the hydraulic piston inside the PTO.

Then, the linearisation of the geometric constraints leads to the linear combination G such that,

$$\begin{cases} x_1 = w_H \\ x_2 = w_P \\ x_3 = w_H - D_{WEC} w_P - \frac{L_{ARM} \cos \theta_{ARM}}{L_2 \cos \theta_2} w_{PTO}, \\ x_4 = w_P + \frac{1}{L_2 \cos \theta_2} w_{PTO} \end{cases} \quad (14)$$

where D_{WEC} is the horizontal distance between the vertical line passing through the centre of the WEC and the vertical line passing through the CoG of the platform.

The contact forces acting on the platform around the hinge point P are evaluated based on f_{PTO_z} and the remaining constraint force acting on the articulated arm, $f_{Q_z} = y$.

Thus, the linear combination H in Eq. (6) is written as

$$\{f_c\} = \begin{Bmatrix} -y \\ M_P + y x_P + f_{PTO}(x_P - x_{PTO}) \\ y \\ 0 \end{Bmatrix}, \quad (15)$$

where M_P is the pitching moment acting on the platform due to the reaction of the binary moment acting on the arm such that the dynamic balance of the arm is satisfied.

Different possibilities exist when modelling the moment M_P and

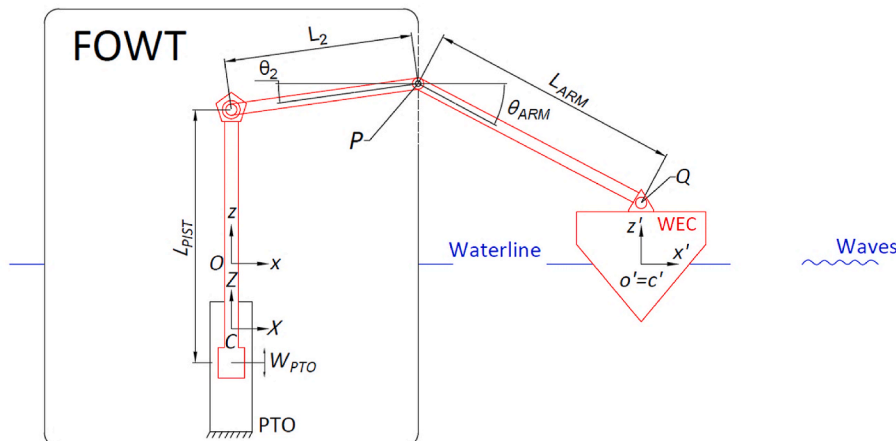


Fig. 1. Schematic drawing of the articulated system. Dimensions are not reproduced in scale.

depend upon the hinge and arm elements: If it is reasonable to consider that the arm rotates freely and frictionless around the hinge and that inertial forces are much lower than PTO and contact forces, then $M_P \cong 0$.

Alternatively, an approximation to account for the friction and the inertial effects is to linearise M_P , as follows,

$$M_P = \delta f_{PTO}(x_P - x_{PTO}) \Rightarrow f_{c2} = \gamma x_P + (1 + \delta) f_{PTO}(x_P - x_{PTO}), \quad (16)$$

where δ is the factor that accounts for the effects of the arm rotating moment on the platform. Clearly, the prior condition $M_P = 0$ is satisfied if $\delta = 0$.

2.7. Linear system and transfer functions

A solution of the hydrodynamic system represented by Eq. (7) is given by

$$\begin{Bmatrix} (W, Y) \cos \psi \\ (W, Y) \sin \psi \end{Bmatrix} = \Lambda^{-1} \begin{Bmatrix} F(\omega) \cos \varphi \\ F(\omega) \sin \varphi \end{Bmatrix}, \quad (17)$$

where

$$\Lambda \equiv \Lambda(\omega) = \begin{bmatrix} C - \omega^2 A(\omega) & -\omega B(\omega) \\ \omega B(\omega) & C - \omega^2 A(\omega) \end{bmatrix}, \quad (18)$$

given that the determinant of Λ is not zero.

Remarkably, for many DOFs, linear solvers are preferable to the inverse matrix calculation expressed in Eq. (17).

The RAOs and RPOs are given, respectively, by

$$(W_j, Y_j) = \sqrt{((W_j, Y_j) \cos \psi_j)^2 + ((W_j, Y_j) \sin \psi_j)^2}, j = 1, \dots, 6N, \quad (19)$$

and

$$\psi_j = \text{atan} \left(\frac{(W_j, Y_j) \sin \psi_j}{(W_j, Y_j) \cos \psi_j} \right), j = 1, 2, \dots, 6N, \quad (20)$$

where the inverse tangent function considers the four quadrants of the Cartesian plane.

The global motion responses are also obtained as complex RAOs simply by combining the complex solutions of Eqs. (19) and (20) according to Eq. (14).

It is also noted that W_{PTO} is a direct output of the method, which reduces uncertainties on the evaluation of wave power absorption.

2.8. Treating the dynamic matrix

If a row of the linear system can be written as a linear combination of other system rows, matrix Λ is singular. However, the symmetric coefficients may not be the same due to computation, in that case the system may be near-singular. The mathematical model based on generalised DOFs and force variables applied to the symmetric FWWP in consideration leads, indeed, to a linear system with twelve rows, where rows of the system can be written as linear combinations of other system rows. In computation, the original system is singular to the working precision of the machine.

It proves necessary to treat the dynamic matrix Λ to obtain numerical convergence. Arguments of symmetry can be considered to eliminate rows of the system, which also depend upon the environmental loads at the right-hand side (RHS). It is also possible to eliminate rows and columns by identifying inactive modes, which reduces computational time, as known as a-priori from single-body hydrodynamics.

In the low-dimensional scenario that neglects the y -direction and considers the surge modes inactive, the DOFs are reduced from 12 (two rigid bodies) to only 3. Moreover, the number of rows in the system is decreased to 4, since one constraint variable remains. The elimination of columns must be performed carefully, for the coefficients of the linear

system on the left-hand side (LHS) are written in generalised modes, but the rows still represent global motions.

First, the elimination of rows is performed by eliminating the eight inactive global modes,

$$\begin{aligned} & \{x_1, x_2, x_3, x_4, x_5, x_6, x_{WEC1}, x_{WEC2}, x_{WEC3}, x_{WEC4}, x_{WEC5}, x_{WEC6}\} \\ & \rightarrow \{x_3, x_5, x_{WEC3}, x_{WEC5}\} \end{aligned}$$

Then, the elimination of columns is performed by selecting the eight generalised modes that are inactive or may be represented as a linear combination,

$$\{x_1, x_2, x_3, x_4, x_5, x_6, w_{PTO}, f_{PTOx}, f_{PTOy}, f_{Qx}, f_{Qy}, f_{Qz}\} \rightarrow \{x_3, x_5, w_{PTO}, f_{Qz}\}$$

The RHS of the equation of motion expresses the environmental loads, and it is now written as

$$\{f_e(\omega)\} = \{f_{e3}(\omega), f_{e5}(\omega), f_{e9}(\omega), f_{e11}(\omega)\}^T. \quad (21)$$

Finally, it is important to note that the system has been decomposed into real and imaginary parts, e.g., Eqs. (17) and (18). Thus, the elimination of matrix Λ rows and columns is performed twice per neglected variable.

2.9. Time domain simulation

The equation of motion (Eq. (7)) can be simulated in the time domain by applying the Cummins formulation (Cummins, 1962),

$$\begin{aligned} [A_\infty] \{(\dot{w}(t), \dot{y}(t))\} &= \{f_e(t)\} - [B_{\text{add}}] \{(\dot{w}(t), \dot{y}(t))\} \\ & - \int_0^\infty [k(\tau)] \{(\dot{w}(t-\tau), \dot{y}(t-\tau))\} d\tau \\ & - [C] \{(\dot{w}(t), \dot{y}(t))\}, \end{aligned} \quad (22)$$

where $A_\infty = \lim_{\omega \rightarrow \infty} \Lambda(\omega)$ includes both rigid-body mass and hydrodynamic added mass, and

$$\kappa_{ij}(\tau) = \frac{2}{\pi} \int_0^\infty \widetilde{B}_{\text{rad}} \cos \omega \tau d\omega, \quad (23)$$

where $\widetilde{B}_{\text{rad}}$ is the part of B accounting for B_{rad} .

Remarkably, it is possible to consider fully nonlinear forces in the RHS of Eq. (22). Moreover, it is straightforward to add nonlinear drag forces into the hydrodynamic model, e.g., using Morison elements (Hallak et al., 2022).

Due to Eq. (11), the presence of constraint variables leads to a matrix A_∞ with at least one column of zeros, meaning that matrix A_∞ has no inverse. To overcome this issue, an adapted matrix \widetilde{A}_∞ is created by adding artificial values in the diagonal of the zero-columns (the last K in A_∞ previously to the treatment), such that matrix \widetilde{A}_∞ is invertible and outputs the same motion responses. On the other hand, the constraint forces are evaluated in the second part of the iteration step, where the exact equation of motion is considered at the same instant to evaluate the force variables. Thus,

$$\begin{aligned} \{(\dot{\theta}(t), \dot{\gamma}(t))\} &= [\widetilde{A}_\infty]^{-1} \left(\{f_e(t)\} - [B_{\text{add}}] \{(\dot{w}(t), \dot{y}(t))\} \right. \\ & \left. - \int_0^T [k(\tau)] \{(\dot{w}(t-\tau), \dot{y}(t-\tau))\} d\tau - [C] \{(\dot{w}(t), \dot{y}(t))\} \right), \end{aligned} \quad (24)$$

where

$$\begin{cases} \Theta = \dot{w}(t) \\ Y = \dot{y}(t) \end{cases}, \quad (25)$$

and the convolution integral in Eq. (24) is performed until instant T , such that the IRFs converge.

Then, force variables are evaluated in a second part within the same iteration step,

$$\begin{aligned} \{Y(t)\} = & [A_\infty]_K^{-1} \left(\{f_e(t)\} - [B_{\text{add}}]_K \{\Theta(t)\} - \int_0^T [k(\tau)]_K \{\Theta(t)\} d\tau \right. \\ & \left. - [C]_K \{w(t)\} \right), \end{aligned} \quad (26)$$

where the index K in $[\]_K$ stands for the block matrix representing the coupling between generalised motions and generalised forces.

2.10. Natural frequencies

An advantage of the analytical formulation is the assessment of the natural frequencies. Hydrodynamic systems are excited by waves that provide oscillatory loads, thus it is important to assess the floating systems' resonant modes of motion. It is noted that the evaluation of the natural frequencies for a floating multi-body geometry with articulated arms still lacks understanding.

Equation (17) shows that if the determinant of the matrix Λ is zero, the response will be spurious. Moreover, the response will oscillate with arbitrarily large amplitudes for arbitrarily small determinant values. Since the determinant of the matrix is a function of the frequency ω , it is reasonable to hypothesise that the system's natural frequencies are the values of ω such that

$$\omega = \omega_{Nj} \Leftrightarrow \{\omega_{Nj} \text{ is the } j\text{-th local minimum of } |\det \Lambda(\omega)| \text{ neglecting the damping terms}\}. \quad (27)$$

This definition is similar to the definition usually considered in classical mechanics (e.g., Fowles and Cassiday, 1962) – that states that ω_N is a natural frequency if, and only if, $|\det \Lambda(\omega_N)| = 0$. In fact, the definition in Eq. (27) is broader, for it includes all "classical" natural frequencies, but, in hydrodynamic systems, because the terms of Λ are functions of the wave frequency, it is possible to observe local minima with near-zero determinants when solving Eq. (27). If the damping terms are not neglected in Eq. (27), the local minima are found at the damped frequencies of the system.

The hypothesis is easily proven to be true for a 1 DOF system: If the equation of motion reads

$$m\ddot{x} + b\dot{x} + cx = F_e(t), \quad (28)$$

where m is the inertia of the system, b is the damping parameter of the system, c is the stiffness parameter of the system, and F_e is the exciting force. Then,

$$\Lambda^* \equiv \Lambda^*(\omega) = \begin{bmatrix} c - \omega^2 m & -\omega b \\ \omega b & c - \omega^2 m \end{bmatrix} \quad (29)$$

$$\Rightarrow \det \Lambda^*(\omega) = \det \begin{bmatrix} c - \omega^2 m & -\omega b \\ \omega b & c - \omega^2 m \end{bmatrix} = (c - \omega^2 m)^2 + (\omega b)^2. \quad (30)$$

Thus, $\det \Lambda^*$ assumes only non-negative values.

Then, if $b = 0$, $\det \Lambda^*(\omega)$ has a single local minimum at the natural frequency ω_N ,

$$b = 0, \omega = \sqrt{c/m} = \omega_N \Rightarrow \det \Lambda^*(\omega_N) = 0. \quad (31)$$

If $b \neq 0$, $\det \Lambda^*(\omega)$ has a single local minimum at the damped frequency ω_D ,

$$b \neq 0, \omega = \sqrt{c/m} \sqrt{1 - b^2/4mc} = \omega_D \Rightarrow \det \Lambda^*(\omega_D) = \min(\det \Lambda^*(\omega)), \quad (32)$$

and the amplitude of response $|X|$ achieves its maximum value for a given excitation force amplitude $|F_e|$,

$$|X| = \frac{|F_e|}{\sqrt{(c - \omega_D^2 m)^2 + (\omega_D b)^2}} = \frac{|F_e|/c}{\sqrt{\xi^4 + (2\xi\omega_D/\omega_N)^2}}, \quad (33)$$

where

$$\xi = b/\sqrt{4mc}, \quad (34)$$

is the damping ratio of the system.

2.11. Analytical natural frequencies of a low-dimensional FWFP

For a floating multi-body geometry with many DOFs, the mathematical identity to find the determinant of a block matrix is useful,

$$\det \begin{bmatrix} \mathbb{D} & \mathbb{E} \\ \mathbb{F} & \mathbb{G} \end{bmatrix} = \det \mathbb{D}^* \det(\mathbb{G} - \mathbb{F}\mathbb{D}^{-1}\mathbb{E}), \quad (35)$$

where \mathbb{D} and \mathbb{G} are square matrixes, and \mathbb{E} and \mathbb{F} are matrixes of adequate size.

Thus, if the damping terms in Eq. (18) are neglected,

$$B(\omega) = \mathbf{0} \Rightarrow |\det \Lambda(\omega)| = \det \Lambda(\omega) = (\det(C - \omega^2 A(\omega)))^2, \quad (36)$$

and the minimum of $|\det \Lambda(\omega)|$ is found at the same frequency as the minimum of

$$|\det(C - \omega^2 A(\omega))|.$$

If it is further considered that $\delta = 0$, as well as $a_{ij}(\omega) \cong a_{ij}$, then,

$$|\det(C - \omega^2 A(\omega))| = \begin{vmatrix} c_{11} - \omega^2 a_{11} & c_{12} - \omega^2 a_{12} & c_{13} - \omega^2 a_{13} & -1 \\ c_{21} - \omega^2 a_{21} & c_{22} - \omega^2 a_{22} & c_{23} - \omega^2 a_{23} & x_p \\ c_{31} - \omega^2 a_{31} & c_{32} - \omega^2 a_{32} & c_{33} - \omega^2 a_{33} & 1 \\ c_{41} - \omega^2 a_{41} & c_{42} - \omega^2 a_{42} & c_{43} - \omega^2 a_{43} & 0 \end{vmatrix} \quad (37)$$

$$\Rightarrow |\det(C - \omega^2 A(\omega))| = 0 \Leftrightarrow P(\omega^2) = 0, \quad (38)$$

where P is a cubic (third-degree) polynomial.

It is known that a cubic polynomial has three distinct real roots if its discriminant Δ_3 is positive,

$$P(\omega^2) = \acute{a}(\omega^2)^3 + \acute{b}(\omega^2)^2 + \acute{c}(\omega^2) + \acute{d} \quad (39)$$

$$\Rightarrow \Delta_3 = 18\acute{a}\acute{b}\acute{c}\acute{d} - 4(\acute{b}^3\acute{d} + \acute{c}^3\acute{a}) + \acute{b}^2\acute{c}^2 - 27\acute{a}^2\acute{d}^2, \quad (40)$$

Then, if $\Delta_3 > 0$, the roots of P are given by



Fig. 2. Perspective view of the hybrid wind-wave platform. (DOI: 10.54499/PTDC/EME-REN/0242/2020).

$$\begin{cases} \omega_1^2 = -\frac{1}{3\hat{a}} \left(\hat{b} + E + \frac{\Delta_0}{E} \right) \\ \omega_2^2 = -\frac{1}{3\hat{a}} \left(\hat{b} - \frac{1+i\sqrt{3}}{2} E - \frac{2\Delta_0}{(1+i\sqrt{3})E} \right), \\ \omega_3^2 = -\frac{1}{3\hat{a}} \left(\hat{b} - \frac{1-i\sqrt{3}}{2} E - \frac{2\Delta_0}{(1-i\sqrt{3})E} \right) \end{cases} \quad (41)$$

where

$$E = \sqrt[3]{\frac{\Delta_1 \pm \sqrt{\Delta_1^2 - 4\Delta_0^3}}{2}}, \quad (42)$$

$$\Delta_0 = \hat{b}^2 - 3\hat{a}\hat{c}, \quad (43)$$

$$\Delta_1 = 2\hat{b}^3 - 9\hat{a}\hat{b}\hat{c} + 27\hat{a}^2\hat{d}. \quad (44)$$

The analytical formulae presented above provide the first estimates of natural frequencies for a constrained floating multi-body system with 3 DOFs.

3. Description of the hybrid platform

The multi-body hybrid system under consideration is presented in Fig. 2. As pictured, the system is designed initially to couple 3 WECs with a FOWT, though the investigation herein conducted considers only the WEC at the front, i.e., the one near the viewer in Fig. 2, to derive a low-dimensional scenario where verification can indeed be accomplished.

Table 1
Adapted OC4 main parameters.

Parameter	Unit	Value
Outer columns' total height	m	40.5
Central column total height	m	40.0
Outer columns distance (center-to-center)	m	66.67
Outer upper column diameter	m	16.00
Outer lower column diameter	m	32.00
Central column diameter	m	8.67
Bracings diameter	m	2.80
Freeboard	m	15.20
Draft	m	26.70
Displacement	ton	32000
CoG z-position	m	-13.46
Radius of gyration R_{xx}	m	24.00
Radius of gyration R_{yy}	m	24.00
Radius of gyration R_{zz}	m	26.00
Heave damping coefficient	-	20%
Pitch damping coefficient	-	40%

Table 2
WEC main parameters.

Parameter	Unit	Value
Diameter	m	8.0
Draft	m	4.0
Displacement	ton	132
CoG z-position	m	0.0
CoG x-position	m	39.25
Radius of gyration R_{xx}	m	2.0
Radius of gyration R_{yy}	m	2.0
Radius of gyration R_{zz}	m	2.0
Heave damping coefficient	-	50%
Pitch damping coefficient	-	25%

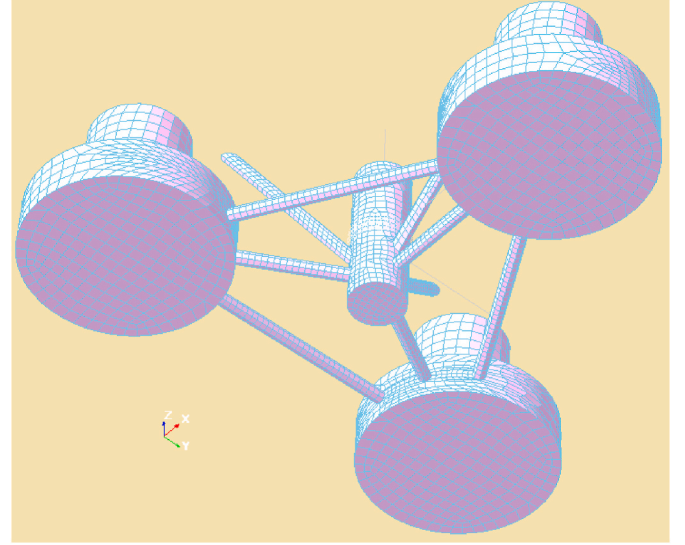


Fig. 3. Underwater mesh of the adapted DeepCWind platform with 6000+ panels.

Table 3
PTO and articulated arm main parameters.

Parameter	Unit	Value
PTO supplementary mass	ton	50.0
PTO damping coefficient	kNs/m	320.0
PTO stiffness coefficient	kN/m	50.0
1st arm's length	m	23.47
1st arm's angle	deg	26.57
2nd arm's length	m	18.27
2nd arm's angle	deg	2.50
Piston z-position	m	-24.0

To be more precise, the FWWP design consists of a version of the OC4 DeepCWind semi-submersible platform (Robertson et al., 2014), adapted to host a 10 MW wind turbine and hemispheric WECs. The main parameters of the platform and WEC are presented in Tables 1 and 2, respectively.

The time domain simulation code is written in Matlab®, whereas the multi-body hydrodynamic coefficients are obtained a priori using SESAM HydroD® and its diffraction and radiation solver Wadam®. Fig. 3 details the mesh used in Wadam® calculations.

An onboard hydraulic PTO is considered, with parameters listed in Table 3. The supplementary mass has been updated and amounts to around 40% of WEC's displacement. The PTO connection and relative constraints are analogous to Fig. 1. The environmental parameters used for the analysis are given in Table 4. Only head waves are considered.

Table 4
Environmental parameters.

Local parameters								
Water depth = 140 m			Water density = 1000 kg/m ³			Gravity = 9.80665 m/s ²		
Regular waves parameters								
Index [-]	Wave Period [s]	Frequency [rad/s]	Index [-]	Wave Period [s]	Frequency [rad/s]	Index [-]	Wave Period [s]	Frequency [rad/s]
1	33.07	0.19	17	9.38	0.67	33	5.46	1.15
2	28.56	0.22	18	8.98	0.70	34	5.32	1.18
3	25.13	0.25	19	8.61	0.73	35	5.19	1.21
4	22.44	0.28	20	8.27	0.76	36	5.07	1.24
5	20.27	0.31	21	7.95	0.79	37	4.95	1.27
6	18.48	0.34	22	7.66	0.82	38	4.83	1.30
7	16.98	0.37	23	7.39	0.85	39	4.72	1.33
8	15.71	0.40	24	7.14	0.88	40	4.62	1.36
9	14.61	0.43	25	6.90	0.91	41	4.52	1.39
10	13.66	0.46	26	6.68	0.94	42	4.42	1.42
11	12.82	0.49	27	6.48	0.97	43	4.33	1.45
12	12.08	0.52	28	6.28	1.00	44	4.24	1.48
13	11.42	0.55	29	6.10	1.03	45	4.16	1.51
14	10.83	0.58	30	5.93	1.06	46	4.08	1.55
15	10.30	0.61	31	5.76	1.09	47	4.00	1.57
16	9.82	0.64	32	5.61	1.12	48	3.93	1.60

4. Results and analysis

4.1. Linear combinations G and H

The linear combinations *G* and *H* are represented by coefficients g_{ij} , h_{ij} and $h_{ij}^{(k)}$. These coefficients must be analytically determined using the proposed modelling method. For any particular geometry, it is necessary to consider the exact definitions of PTOs, mechanical connections, and WEC arrangement to evaluate these coefficients. The values obtained for the low-dimensional case study under analysis are presented in Tables 5 and 6. The coordinates are written about the global, right-handed O_{xyz} reference frame unless specified otherwise.

Table 5
Coefficients of linear combination *G* (transform between global motions and variables).

g_{ij}	Variable (w_j, y_j)						
	1		2		3		4
	w_H	w_P	w_{PTO}	w_H	w_P	w_{PTO}	y
Global motion (x_i)	1	x_1	1	0	0	0	0
	2	x_2	0	1	0	0	0
	3	x_3	1	$-D_{WEC}$	$-L_{ARM} \cos(\theta_{ARM})/L_2 \cos(\theta_2)$	0	0
	4	x_4	0	1	$1/L_2 \cos(\theta_2)$	0	0

Table 6
Coefficients of linear combination *H* (constraint forces).

$h_{ij}^{(k)}$	Variable (w_j, y_j)						
	3, k = 0		3, k = 1		3, k = 2		4
	w_{PTO}	w'_{PTO}	w_{PTO}	w'_{PTO}	w''_{PTO}	y	
Global motion (x_i)	1	x_1	0	0	0	-1	
	2	x_2	$\kappa(x_p - x_{PTO})$	$\beta(x_p - x_{PTO})$	$\mu(1 + \delta)(x_p - x_{PTO})$	x_p	
	3	x_3	0	0	0	1	
	4	x_4	0	0	0	0	

4.2. Dynamic response

The RAOs and RPOs of the many modes of the system are direct outputs of the method. First, Figs. 4 and 5 present the FWWP RAOs and RPOs in heave and pitch, respectively.

It is clear from Fig. 4 that the addition of hydrodynamic coupling, namely, due to the presence of the WEC in the FOWT surroundings, does not significantly affect the FWWP heave RAO, even though heave motion is damped in the range between 0.40 and 0.60 rad/s. This change is raised by the difference in phase between heave motion and incoming wave, as clear from the heave RPOs. In the low-frequency range, the FWWP rides the wave, and the heave RAO tends to 1.0 m/m, as expected, which also holds for the fully coupled hybrid system.

It is also important to note that the fully coupled FWWP heaves slightly more than the single-body FOWT in the whole frequency range, with some amplification around the heave natural frequency $\omega \approx 0.32$ rad/s.

In opposition to the heave effects, Fig. 5 shows that the platform pitch motion is amplified in the fully coupled scenario, whereas the hydrodynamic coupling accounts for a minor influence on the dynamic interaction. The effect is more pronounced around the FOWT pitch resonant frequency ($\omega \approx 0.25$ rad/s). It seems that a new mode appears around 0.90–0.95 rad/s, which also appeared in a less pronounced way in the heave RAO (Fig. 4). By comparing the pitch RPOs, it is clear that the mechanical coupling considerably affects the phase difference between incoming wave and pitch motion, whereas the single-body FOWT and fully coupled FWWP are out-of-phase throughout practically the whole frequency range. The difference is even more significant near the pitch resonant frequency, an essential factor for pitch amplification observed in the hybrid platform.

It is important to note that the single-WEC arrangement considered in the fully coupled scenario may negatively affect the pitch responses, shown in Fig. 5, due to an asymmetric lever effect.

Fig. 6 presents WEC's heave RAO, the piston motion response, and the main force variables of the system, namely, the generalised force (equals the vertical force acting on the WEC) and the piston force. The curves are drawn for the fully coupled scenario, i.e., the only scenario where the PTO is in operation.

Because the WEC is much smaller than the FOWT, the coupling effect

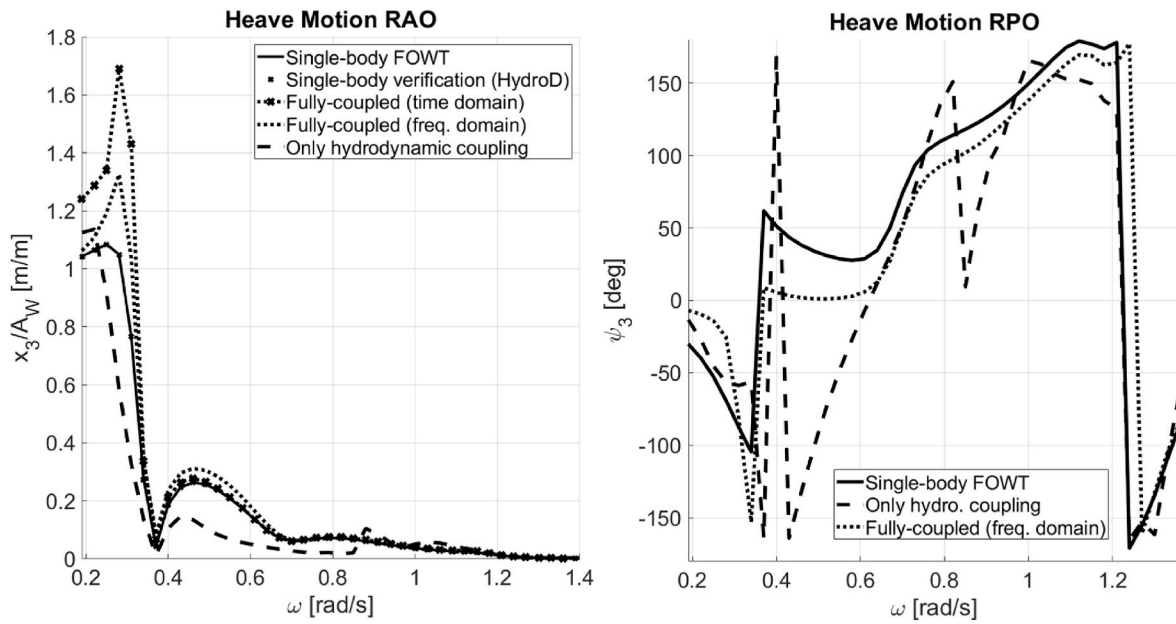


Fig. 4. Heave motion RAOs (left) and RPOs (right).

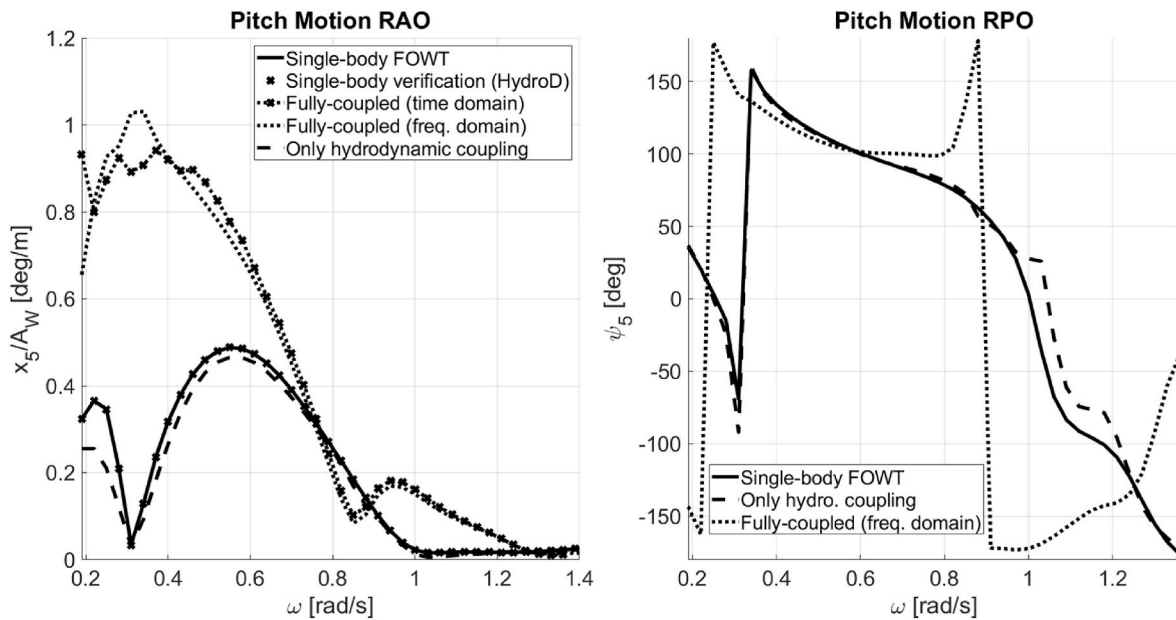


Fig. 5. Pitch motion RAOs (left) and RPOs (right).

is stronger at the WEC. That is clear from the amplitude of motion of the WEC, as shown in Fig. 6: The model predicts that the WEC heaves up to 2.6 m amplitude for unit amplitude waves. The high amplitude of motion is related to the constructive interference between global heave, global pitch and piston motions. The motion amplitude within the PTO is at a maximum of 1.4 m, which fulfils maximum stroke requirements. However, it indicates that attention must be directed to the stroke requirements, especially in harsh sea states.

Fig. 6 also shows that the constraint force transfer function varies with the frequency, reaching up to 640 MN per meter of incoming wave. The PTO force lies in the same order of magnitude, though it is smaller in the low-frequency range and higher in the high-frequency range, reaching a maximum of around 300 MN at 1.2 rad/s. This observation is consistent with the previous findings of Babarit et al. (2012).

4.3. Wave energy conversion

Fig. 7 presents results regarding wave energy absorption for unit-amplitude waves and the WEC's capture width. The amount of power absorbed by the WEC in the hybrid platform is more significant than that of state-of-the-art point absorbers, for it generates energy throughout the whole frequency range. Indeed, several peaks of wave power are found in Fig. 7, whereas the highest peak is seen at 1.2 rad/s (also when the PTO force is at maximum), absorbing more than 70 kW for a unit-amplitude incoming wave.

From left to right, the first peak corresponds to the FWFP heave natural frequency, the second corresponds to the piston natural frequency, and the last corresponds to the WEC's heave natural frequency. A first approximation for the piston's natural frequency is given by $\omega_{PTO} \cong \sqrt{\kappa/(\mu + M_{WEC})}$, where M_{WEC} is the inertia of the WEC, including its added mass. Thus, $\omega_{PTO} \cong 0.52$ rad/s.

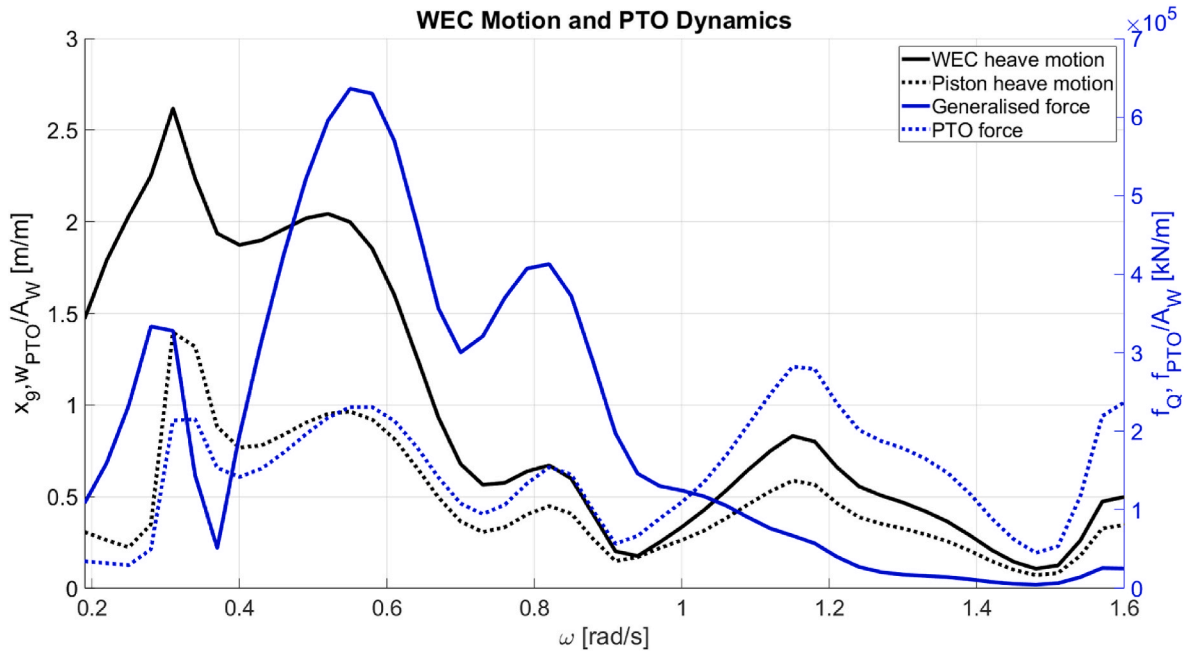


Fig. 6. WEC and PTO motions for unit-amplitude incoming waves in the fully coupled scenario.

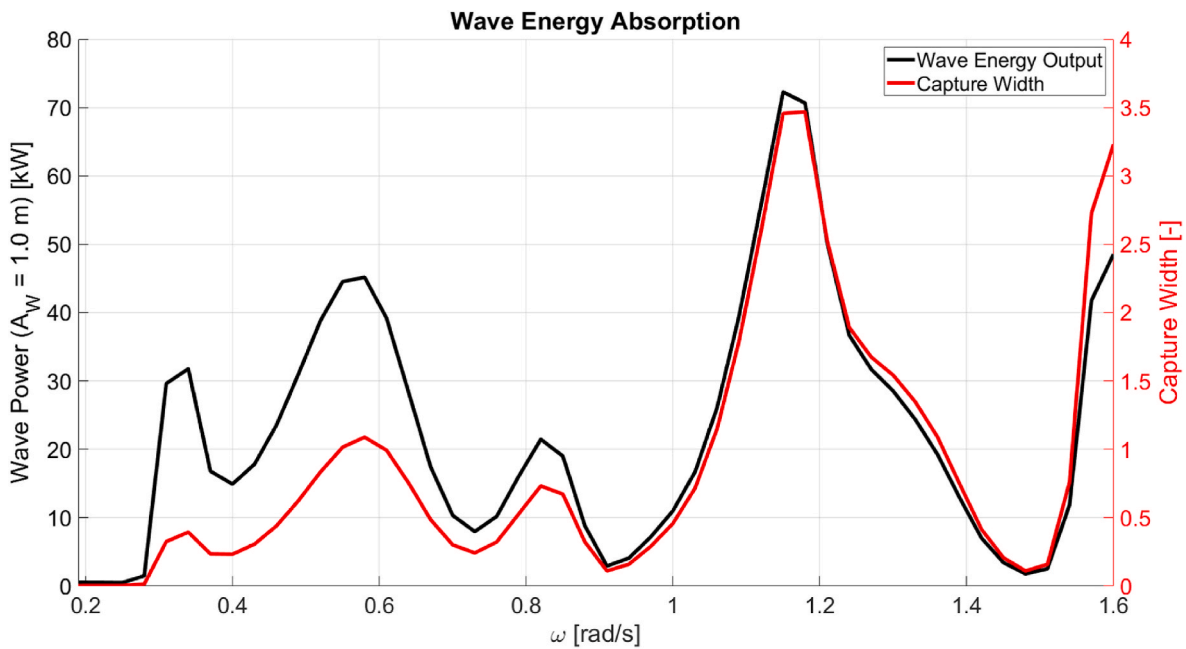


Fig. 7. Performance of the Wave Energy Converter coupled with the adapted DeepCWind platform.

Within the frequency range between 0.30 and 0.60 rad/s, i.e., equivalent to waves from 10 to 21 period seconds (usual band of sea waves), the amount of absorbed wave power is 30 kW for unit-amplitude waves, and the capture width is around 1. Capture width increases in the high-frequency range, with two peaks of around 3.5.

By comparing Figs. 5 and 7, it is clear that pitch amplification and wave power absorption effects are dissociated. The first happens in the low-frequency range and the latter in the high-frequency range. An FWWP with a symmetric WEC arrangement and optimal PTO system should use this observation to restrict pitch motions without losing WECs' efficiency. In addition, the results shown in Fig. 6 also point out that stroke requirements shall be fulfilled in this scenario, though the PTO forces shall continue to be high overall.

4.4. Natural frequencies

The hypothesis that the minimum of the determinant of matrix Λ is related to the natural and damped frequencies of floating constrained multi-body systems is investigated in this sub-section. Analytical results are drawn by solving Eqs. (38)–(44), whereas numerical results of natural and damped frequencies are obtained by solving the minimum determinant of $\Lambda(\omega)$. The natural and damped frequencies can also be compared with the maxima observed in the RAOs (Figs. 4–6).

The single-body FOWT and single-body WEC present natural frequencies that are known apriori, namely, 1.81 rad/s and 0.26 rad/s for the WEC's heave and pitch modes, respectively, and 0.32 rad/s and 0.25 rad/s for the FOWT's heave and pitch modes, respectively. Those values

are matched when applying the minimum determinant method to the single-body matrixes.

The minimum determinant method also calculates the damped frequencies for the hydrodynamically coupled system. The damped frequencies are equivalent to the single-body FOWT natural frequencies, namely, 0.32 rad/s and 0.25 rad/s, meaning that the FOWT coefficients rule over the WEC coefficients. Therefore, it can be concluded that the resonant modes of motion of the hydrodynamically coupled system approach the FOWT resonant modes of motion. On the other hand, the minimum determinant method outputted the fully coupled FWFP damped frequencies as 0.49 rad/s and 0.25 rad/s, i.e., the main resonant modes may differ after considering the geometric and mechanical constraints. The first frequency practically corresponds with the piston's natural frequency; again, $\omega_{PTO} \cong \sqrt{\kappa/(\mu + M_{WEC})} = 0.52 \text{ rad/s}$.

Because semi-submersible designs effectively reduce wave loads at the resonant modes, the abovementioned values do not necessarily correspond with the maxima of motion response (Figs. 4–6). The main exception is the significant pitch amplification, near the pitch natural frequency for the fully-coupled system, which may be related to the single-WEC arrangement that negatively affects the pitch response due to a strong lever effect.

By applying the analytical formulae for the 3 DOF-constrained system, three natural frequencies are found: in ascending order, they correspond to 0.18, 0.25 and 0.49 rad/s. The latter frequency appears to correspond to the piston's natural frequency, and the middle one corresponds with the pitch's natural frequency, both matching the values found by the minimum determinant method. The lowest natural frequency must be related to some coupled mode of motion, for it differs from the other known modes and is located in the low-frequency range. It may also be approximated due to the approximation of hydrodynamic added mass (Eq. (37)) and zero damping assumption. Whereas the minimum determinant method considers damping forces – not accounted in the analytical formulae –, and given the motion responses presented in Figs. 4–6, it is suggested that this low-frequency mode is mitigated by damping and phase effects.

5. Conclusions

In this paper, the formulation to simulate and analyse floating constrained multi-body systems was developed further and now includes formulae to obtain the natural and damped frequencies of complex hydrodynamic systems. By selecting a hybrid system consisting of a semi-submersible FOWT coupled with a point absorber WEC using a PTO system and articulated arm, it is proven that the new formulation and method can be adopted for the simulation of nonlinear floating multi-body systems, which has direct application in the development of new hybrid wind-wave technologies.

The results shown in this paper prove that the minimum determinant method is a consistent method to devise the natural and damped frequencies of floating constrained multi-body systems, and also that the analytical formulation can be used for a 3 DOF multi-body system. While the hydrodynamically coupled system's natural frequencies approach the single-body natural frequencies because the FOWT coefficients rule over the WEC coefficients, the piston natural frequency is a particular frequency of the fully coupled FWFP found by both the analytical method and the minimum determinant method. Naturally, it is also noted that the piston frequency corresponds to around 12 s of period, which is usually within the most energetic bands of ocean waves, also corresponding to a peak of wave power absorption.

The results also consist of force and motion responses for FOWT and WEC in the hybrid configuration and performance parameters regarding wave energy conversion and the PTO response. The results indicate that the hybrid platform under consideration moves within a reasonable

range, the heave motion being hardly modified, whereas the pitch motion is amplified around the resonance, an observation conditioned by the single-WEC arrangement used for verification. The WEC may heave considerably within the frequency band 0.2–0.7 rad/s; however, the WEC absorbs a significant amount of wave energy throughout almost the whole range of wave frequencies, reaching more than 70 kW of absorbed power for a unit-amplitude wave and has typically better performance in the high-frequency range, reaching a capture width value of 3.5. In the fully coupled scenario, the three active DOFs (heave, pitch and piston) contribute positively to the large WEC response, which was proven by the phase difference of the RPOs. It is important to remark that the effects of pitch amplification at the resonance and the increase in wave power absorption are dissociated.

Though the PTO coefficients lie within rational values (da Silva et al., 2022), the order of magnitude of the PTO force is high overall ($>10^5 \text{ kN}$) and even smaller than the constraint force acting on the WEC-arm interface. Nevertheless, the PTO easily fulfils maximum stroke requirements for unit-amplitude waves.

It is important to note that the verification case was selected based on the low-dimensional scenario it represents. At the same time, the hybrid FWFP would consist of the FOWT plus three symmetric WECs around the platform. Due to symmetry, the actual system shall present a better pitch response and reduced WEC motion.

Last but not least, the novel formulation for analysing floating constrained multi-body systems may be applied in more in-depth studies, encompassing concept optimisation or new control strategies. The formulation may be also applied to other floating systems, such as the constrained WEC arrays and aquaculture systems.

CRedit authorship contribution statement

Thiago S. Hallak: Writing – original draft, Visualization, Methodology, Formal analysis. **José F. Gaspar:** Writing – review & editing, Conceptualization. **C. Guedes Soares:** Writing – review & editing, Supervision.

Declaration of competing interest

The authors declare that they have no known competing financial interests or personal relationships that could have appeared to influence the work reported in this paper.

Acknowledgements

The first author has a PhD Scholarship from the Portuguese Foundation for Science and Technology (Fundação para a Ciência e Tecnologia – FCT), under contract SFRH/BD/145602/2019. This work contributes to the Strategic Research Plan of the Centre for Marine Technology and Ocean Engineering (CENTEC), which is financed by the Portuguese Foundation for Science and Technology (Fundação para a Ciência e Tecnologia - FCT) under contract UIDB/UIDP/00134/2020, and the project "Variable geometry Wave Energy Conversion system for floating platforms" funded by FCT under contract PTDC/EME-REN/0242/2020 (DOI: <https://doi.org/10.54499/PTDC/EME-REN/0242/2020>).

References

- Asai, T., Tsukamoto, S., Nemoto, Y., Yoshimizu, K., Watanabe, U., Taniyama, Y., 2024. Numerical simulation of a floating offshore wind turbine incorporating an electromagnetic inerter-based device for vibration suppression and wave energy conversion. *Struct. Control Health Monit.*, 5513733 <https://doi.org/10.1155/2023/5513733>.

- Babarit, A., Hals, J., Muliawan, M.J., Kurniawan, A., Moan, T., Krokstad, J., 2012. Numerical benchmark study of a selection of wave energy converters. *Renew. Energy* 41, 44–63. <https://doi.org/10.1016/j.renene.2011.10.002>.
- Balitski, P., Bacelli, G., Ringwood, J.V., 2014. Control-influenced layout optimisation of arrays of wave energy devices. In: *Proc. ASME 2014 33rd Int. Conf. Ocean Offshore Arct. Eng.*, San Francisco, CA, USA, OMAE2014-24136. <https://doi.org/10.1115/OMAE2014-24136>.
- Budal, K., 1977. Theory of absorption of wave power by a system of interacting bodies. *J. Ship Res.* 21 (4), 248–254. <https://doi.org/10.5957/jsr.1977.21.4.248>.
- Chakrabarti, S.K., 1999. Response of multiple structures including interaction. In: *Proc. 3rd Int. Workshop on Very Large Floating Structures VLFS '99*, Honolulu, HI, USA, vol. II, pp. 792–804.
- Chakrabarti, S., 2000. Hydrodynamic interaction forces on multi-modulated structures. *J. Ship Res.* 21 (4), 1037–1063. [https://doi.org/10.1016/S0029-8018\(99\)00034-7](https://doi.org/10.1016/S0029-8018(99)00034-7).
- Chen, M., Wang, R., Xiao, P., Zhu, L., Li, F., Sun, L., 2020. Numerical analysis of a floating semi/submersible wind turbine integrated with a point absorber wave energy converter. *Proc. ISOPE 2020 13th Int. Conf. Ocean Polar Eng. Conf.* 300–307.
- Chen, M., Ouyang, M., Guo, H., Zuo, M., Zhang, C., 2023. A coupled hydrodynamic-structural model for flexible interconnected multiple floating bodies. *J. Mar. Sci. Eng.* 11, 813. <https://doi.org/10.3390/jmse11040813>.
- Chen, M., Ding, J., Yang, Y., Zhou, H., Tao, T., Liu, S., Sun, L., Hua, L., 2024. Performance analysis of a floating wind/wave power generation platform in operational sea-state. *J. Mar. Sci. Eng.* 12, 206. <https://doi.org/10.3390/jmse12020206>.
- Chen, Z., Yu, J., Sun, J., Tan, M., Yang, S., Ying, Y., Qian, P., Zhang, D., Si, Y., 2022. Load reduction of semi-submersible floating wind turbines by integrating heaving-type wave energy converters with bang-bang control. *Front. Energy Res.* 10, 929307. <https://doi.org/10.3389/fenrg.2022.929307>.
- Child, B.F.M., Venugopal, V., 2010. Optimal configurations of wave energy device arrays. *Ocean Eng.* 37 (16), 1402–1417. <https://doi.org/10.1016/j.oceaneng.2010.06.010>.
- Cummins, W.E., 1962. The impulse response function and ship motions. *Schiffstechnik* 47, 101–109.
- Diaz, H.M., Guedes Soares, C., 2020. Review of the current status, technology and future trends of offshore wind farms. *Ocean Eng.* 209, 107381. <https://doi.org/10.1016/j.oceaneng.2020.107381>.
- Diaz, H.M., Serna, J., Nieto, J., Guedes Soares, C., 2022. Market needs, opportunities and barriers for the floating wind industry. *J. Mar. Sci. Eng.* 10 (7), 934. <https://doi.org/10.3390/jmse10070934>.
- Falnes, J., 1980. Radiation impedance matrix and optimum power absorption for interacting oscillators in surface waves. *Appl. Ocean Res.* 2 (2), 75–80. [https://doi.org/10.1016/0141-1187\(80\)90032-2](https://doi.org/10.1016/0141-1187(80)90032-2).
- Fitzgerald, C., Thomas, G., 2007. A preliminary study on the optimal formation of an array of wave power devices. In: *Proc. EWTEC 2007 7th European Wave Tidal Energy Conf.*, Porto, Portugal.
- Fowles, G.R., Cassiday, G.L., 1962. *Analytical Mechanics*, seventh ed. Thomson Brooks/Cole, Belmont, CA, USA.
- Gao, Q., Bechlenberg, A., Jayawardhana, B., Ertugrul, N., Vakis, A.I., Ding, B., 2024. Techno-economic assessment of offshore wind and hybrid wind/wave farms with energy storage systems. *Renew. Sust. Energy Rev.* 192, 114263. <https://doi.org/10.1016/j.rser.2023.114263>.
- Gaspar, J.F., Kamarlouei, M., Sinha, A., Xu, H., Calvário, M., Fay, F.X., Robies, E., Guedes Soares, C., 2017. Analysis of electrical drive speed control limitations of a power take-off system for wave energy converters. *Renew. Energy* 113, 335–346. <https://doi.org/10.1016/j.renene.2017.05.085>.
- Ghafari, H.R., Ghassemi, H., He, G., 2021. Numerical study of the Wavestar wave energy converter with multi-point-absorber around DeepCWind semi-submersible floating platform. *Ocean Eng.* 232, 109177. <https://doi.org/10.1016/j.oceaneng.2021.109177>.
- Ghafari, H.R., Ghassemi, H., Neisi, A., 2022. Power matrix and dynamic response of the hybrid Wavestar-DeepCWind platform under different diameters and regular wave conditions. *Ocean Eng.* 247, 110734. <https://doi.org/10.1016/j.oceaneng.2022.110734>.
- GWEC – Global Wind Energy Council, 2024. Global wind report. Available online. <http://gwec.net/global-wind-report-2024/>. (Accessed 8 July 2024).
- Hallak, T.S., Karmakar, D., Guedes Soares, C., 2021. Hydrodynamic performance of semi-submersible FOWT combined with point-absorber WEC. *Developments in Maritime Technology and Engineering*. CRC Press, pp. 577–585. <https://doi.org/10.1201/9781003216599-61>.
- Hallak, T.S., Guedes Soares, C., Sainz, O., Hernández, S., Arévalo, A., 2022. Hydrodynamic analysis of the WIND-bos spar floating offshore wind turbine. *J. Mar. Sci. Eng.* 10 (12), 1824. <https://doi.org/10.3390/jmse10121824>.
- Hallak, T.S., Gaspar, J.F., Guedes Soares, C., 2023. Dynamic simulation of wave point absorbers connected to a central floating platform. *Proc. EWTEC 2023 European Wave and Tidal Energy Conf.* 15, 496. <https://doi.org/10.36688/ewtec-2023-496>.
- Hallak, T.S., Guedes Soares, C., 2024. An overview of the recent developments in hybrid floating wind-wave platforms. *J. Mar. Sci. Appl.* 23. <https://doi.org/10.1007/s11804-024-00544-w>.
- Hu, J., Zhou, B., Vogel, C., Liu, P., Willden, R., Sun, K., Zang, J., Geng, J., Jin, P., Cui, L., Jiang, B., Collu, M., 2020. Optimal design and performance analysis of a hybrid system combining a floating wind platform and wave energy converters. *Appl. Energy* 269, 114998. <https://doi.org/10.1016/j.apenergy.2020.114998>.
- Kamarlouei, M., Gaspar, J.F., Calvário, M., Hallak, T.S., Mendes, M.J.G.C., Thiebaud, F., Guedes Soares, C., 2020. Experimental analysis of wave energy converters concentrically attached on a floating offshore platform. *Renew. Energy* 152, 1171–1185. <https://doi.org/10.1016/j.renene.2020.01.078>.
- Kamarlouei, M., Gaspar, J.F., Calvário, M., Hallak, T.S., Mendes, M.J.G.C., Thiebaud, F., Guedes Soares, C., 2022. Experimental study of wave energy converter arrays adapted to a semi-submersible wind platform. *Renew. Energy* 188, 145–163. <https://doi.org/10.1016/j.renene.2022.02.014>.
- Kara, F., 2020. Multi-body interactions of floating bodies with time-domain predictions. *J. Waterway Port Coast. Ocean Eng.* 146 (5), 04020031. [https://doi.org/10.1061/\(ASCE\)WW.1943-5460.0000588](https://doi.org/10.1061/(ASCE)WW.1943-5460.0000588).
- Li, L., Gao, Y., Yuan, Z., Day, S., Hu, Z., 2018. Dynamic response and power production of a floating integrated wind, wave and tidal energy system. *Renew. Energy* 116, 412–422. <https://doi.org/10.1016/j.renene.2017.09.080>.
- Liu, Z.C., Guedes Soares, C., 2023. Sensitivity analysis of a numerical model of the dynamics of gravity cages subjected to current and waves. *Ocean Engineering* 287, 115715. <https://doi.org/10.1016/j.oceaneng.2023.115715>.
- Mavrakos, S.A., 1991. Hydrodynamic coefficients for groups of interacting vertical axisymmetric bodies. *Ocean Eng.* 18 (5), 485–515. [https://doi.org/10.1016/0029-8018\(91\)90027-N](https://doi.org/10.1016/0029-8018(91)90027-N).
- Mavrakos, S.A., McIver, P., 1997. Comparison of methods for computing hydrodynamic characteristics of arrays of wave power devices. *Appl. Ocean Res.* 19, 283–291. [https://doi.org/10.1016/S0141-1187\(97\)00029-1](https://doi.org/10.1016/S0141-1187(97)00029-1).
- Mavrakos, S.A., Kalofonos, A., 1997. Power absorption by arrays of interacting vertical axisymmetric wave energy devices. *J. Offshore Mech. Arct. Eng.* 119 (4), 244–251. <https://doi.org/10.1115/1.2829103>.
- McIver, P., 1994. Some hydrodynamic aspects of arrays of wave-energy devices. *Appl. Ocean Res.* 16, 61–69. [https://doi.org/10.1016/0141-1187\(94\)90003-5](https://doi.org/10.1016/0141-1187(94)90003-5).
- Mohapatra, S.C., Bernardo, T.A., Guedes Soares, C., 2021. Dynamic wave induced loads on a moored flexible cylindrical net cage with analytical and numerical model simulations. *Appl. Ocean Res.* 110, 102591.
- Newman, J.N., 1977. *Marine Hydrodynamics*. The MIT Press, Cambridge MA & London UK.
- Newman, J.N., 1994. Wave effects on deformable bodies. *Appl. Ocean Res.* 16 (1), 47–59. [https://doi.org/10.1016/0141-1187\(94\)90013-2](https://doi.org/10.1016/0141-1187(94)90013-2).
- Newman, J.N., 2001. Wave effects on multiple bodies. *Hydrodyn. Ship Ocean Eng.* 3, 3–26.
- Ohkusu, M., 1969. On the heaving motion of two circular cylinders on the surface of a fluid. *Reports of Research Institute for Applied Mechanics*, XVII 58, 167–185.
- Ohkusu, M., 1970. On the Motion of Multihull Ship in Waves, vol. 40. *Society of Naval Architects of West Japan*, pp. 19–47.
- Robertson, A., Jonkman, J.M., Masciola, M., Song, H., Goupee, A., Coulling, A., Luan, C., 2014. Definition of the semi-submersible floating system for Phase II of OC4. *Nat. Renew. Energy Lab. NREL/TP-5000-60601* <https://www.nrel.gov/docs/fy14osti/60601.pdf>. (Accessed 15 September 2024).
- Si, Y., Chen, Z., Zeng, W., Sun, J., Zhang, D., Ma, X., Qian, P., 2021. The influence of power take-off control on the dynamic response and power output of combined semi-submersible floating wind turbine and point-absorber wave energy converters. *Ocean Eng.* 227, 108835. <https://doi.org/10.1016/j.oceaneng.2021.108835>.
- da Silva, L.S.P., Sergiienko, N.Y., Cazzolato, B., Ding, B., 2022. Dynamics of hybrid offshore renewable energy platforms: heaving point absorbers connected to a semi-submersible Floating Offshore Wind Turbine. *Renew. Energy* 199, 1424–1439. <https://doi.org/10.1016/j.renene.2022.09.014>.
- Sinha, A., Karmakar, D., Guedes Soares, C., 2016a. Hydrodynamic performance of concentric arrays of point absorbers. *International Journal of Ocean and Climate Systems* 7 (3), 88–94.
- Sinha, A., Karmakar, D., Guedes Soares, C., 2016b. Performance of optimally tuned arrays of heaving point absorbers. *Renew. Energy* 92, 517–531. <https://doi.org/10.1016/j.renene.2016.02.043>.
- Skene, D.M., Sergiienko, N., Ding, B., Cazzolato, B., 2021. The prospect of combining a point absorber wave energy converter with a floating offshore wind turbine. *Energies* 14, 7385. <https://doi.org/10.3390/en14217385>.
- Stansby, P., Li, G., 2024. A wind semi-sub platform with hinged floats for omnidirectional swell wave energy conversion. *J. Ocean Eng. Mar. Energy*. <https://doi.org/10.1007/s40722-024-00321-5>.
- Teixeira-Duarte, F., Ramos, V., Rosa-Santos, P., Taveira-Pinto, F., 2024. Multi-objective decision tool for the assessment of co-located wave-wind offshore floating energy parks. *Ocean Eng.* 292, 116449. <https://doi.org/10.1016/j.oceaneng.2023.116449>.
- Tuck, E.O., Newman, J.N., 1974. *Hydrodynamic Interactions between Ships*. *Proc. 10th Symposium on Naval Hydrodynamics*, Cambridge, MA, USA, pp. 35–70.
- Wan, L., Gao, Z., Moan, T., 2015. Experimental and numerical study of hydrodynamic responses of a combined wind and wave energy converter concept in survival modes. *Coast. Eng.* 104, 151–169. <https://doi.org/10.1016/j.coastaleng.2015.07.001>.
- Wan, L., Gao, Z., Moan, T., Lugni, C., 2016. Experimental and numerical comparisons of hydrodynamic response for a combined wind and wave energy converter concept under operational conditions. *Renew. Energy* 93, 87–100. <https://doi.org/10.1016/j.renene.2016.01.087>.
- Wu, H., Zhu, F., Yuan, Z., 2024. Effects of WEC shape on the performance of a novel hybrid WEC-FOWT system. *Energy* 288, 129907. <https://doi.org/10.1016/j.energy.2023.129907>.
- Xu, C., Zhou, X.Q., Ren, H.L., Sutulo, S., Guedes Soares, C., 2024. Real-time calculation of ship to ship hydrodynamic interaction in shallow waters with adaptive mesh refinement. *Ocean Engineering* 295, 116943.

- Yeung, R.W., 1978. On the interactions of slender ships in shallow water. *J. Fluid Mech.* 85 (1), 143–159. <https://doi.org/10.1017/S0022112078000567>.
- Zhao, X., Du, X., Li, M., Götteman, M., 2021. Semi-analytical study on the hydrodynamic performance of an interconnected floating breakwater-WEC system in presence of the seawall. *Appl. Ocean Res.* 109, 102555. <https://doi.org/10.1016/j.apor.2021.102555>.
- Zhao, X., Xue, F., Chen, L., Götteman, M., Han, D., Geng, J., Sun, S., 2023. Hydrodynamic analysis of a floating platform coupled with an array of oscillating bodies. *Ocean Eng.* 287, 115439. <https://doi.org/10.1016/j.oceaneng.2023.115439>.
- Zhou, L., Abdelwahab, H.S., Guedes Soares, C., 2021. Experimental and CFD investigation of the effects of a high-speed passing ship on a moored container ship. *Ocean Eng.* 228, 108914. <https://doi.org/10.1016/j.oceaneng.2021.108914>.
- Zhu, K., Shi, H., Zheng, S., Michele, S., Cao, F., 2023. Hydrodynamic analysis of hybrid system with wind turbine and wave energy converter. *Appl. Energy* 350, 121745. <https://doi.org/10.1016/j.apenergy.2023.121745>.